MNRAS **000**, 1–3 (2019) Preprint 17 September 2019 Compiled using MNRAS LATEX style file v3.0

Cassini State Capture

Yubo Su[1], Dong Lai[1]
[1] *Cornell Center for Astrophysics and Planetary Science, Department of Astronomy, Cornell University, Ithaca, NY 14853, USA*

Accepted XXX. Received YYY; in original form ZZZ

ABSTRACT
Abstract

Key words: planet–star interactions

1 INTRODUCTION

2 EQUATIONS

Denote $\vec{S}$ spin of planet, $\vec{l}$ angular momentum of planet, and $\vec{l}_d$ angular momentum of the surrounding disc. We approximate $S \ll L \ll L_d$, so $\vec{l}_d$ is approximately constant. Much of this treatment borrows from (Anderson & Lai 2018). We consider equations in the corotating frame

$$\frac{\mathrm{d}\hat{s}}{\mathrm{d}t} = \omega_{sl}\left(\hat{s}\cdot\hat{l}_d\right)\left(\hat{s}\times\hat{l}_d\right), \tag{1}$$

$$\frac{\mathrm{d}\hat{l}}{\mathrm{d}t} = \omega_{ld}\left(\hat{l}\cdot\hat{l}_d\right)\left(\hat{l}\times\hat{l}_d\right), \tag{2}$$

$$\omega_{sl} = \frac{3k_q}{2k}\left(\frac{R_1}{a_1}\right)^3 S, \tag{3}$$

$$\omega_{ld} = \dots. \tag{4}$$

(TODO get ω_{ld} from Millhollard & Batygin).

We go to the corotating frame with $\vec{l}$ such that it is also fixed in time. The evolution of $\hat{s}$ in this corotating frame is governed by:

$$\frac{\mathrm{d}\hat{s}}{\mathrm{d}t} = \alpha\left(\hat{s}\cdot\hat{l}\right)\left(\hat{s}\times\hat{l}\right) - |g|\left(\hat{s}\times\hat{l}_d\right). \tag{5}$$

$\alpha = \omega_{sd} > 0, g \equiv -\omega_{ld} < 0$ follow traditional sign conventions.

We divide through by α and define parameter η and nondimensionalized time τ

$$\eta \equiv \frac{|g|}{\alpha}, \tag{6}$$

$$\tau \equiv \alpha t. \tag{7}$$

Following Millholland & Batygin (2019), we allow g to vary in time owing to a disk with decaying mass

$$M_d(t) = M_d(0)e^{-t/t_d}. \tag{8}$$

As α is held constant, this equates to η decaying as $\frac{\mathrm{d}\eta}{\mathrm{d}t} = -\frac{\eta}{t_d}$ for some decay time t_η. We nondimensionalize by defining $\epsilon \equiv \frac{1}{\alpha t_\eta}$, so

$$\frac{\mathrm{d}\eta}{\mathrm{d}\tau} = -\epsilon\eta. \tag{9}$$

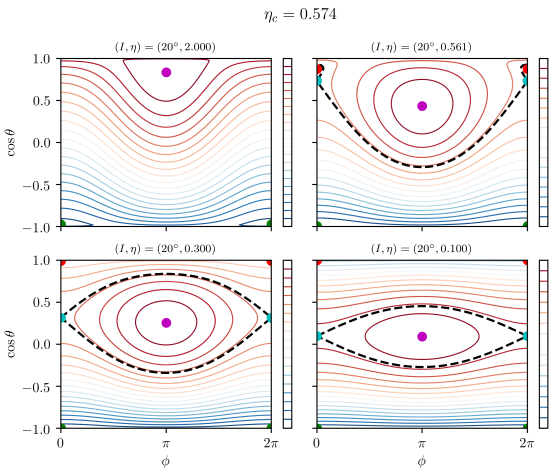

Figure 1. Contour plot of $H(\phi, \cos\theta)$. Black dotted line is the separatrix, which only exists for $\eta < \eta_c$.

2.1 Cassini States

The Cassini state Hamiltonian in the frame corotating with $\hat{l}_d$ about $\hat{l}$ is:

$$H = -\frac{1}{2}\left(\hat{s}\cdot\hat{l}\right)^2 + \eta\left(\hat{s}\cdot\hat{l}_d\right). \tag{10}$$

Spin states satisfying $\frac{\mathrm{d}\hat{s}}{\mathrm{d}t} = 0$ are referred to as *Cassini States* (CS). When $\eta < \eta_c$, there are four CSs, and when $\eta > \eta_c$ there are only two; η_c is (Henrard & Murigande 1987; Ward & Hamilton 2004)

$$\eta_c \equiv \left(\sin^{2/3} I + \cos^{2/3} I\right)^{3/2}. \tag{11}$$

CSs 1, 2, 3 are stable while CS4 is unstable. A contour plot of $H(\phi, \cos\theta)$ is

2.2 Separatrix

In the four-CS regime, one of the CSs is a saddle point, conventionally denoted Cassini State 4 (CS4). All trajectories are periodic with finite period except two critical trajectories asymptotic in the

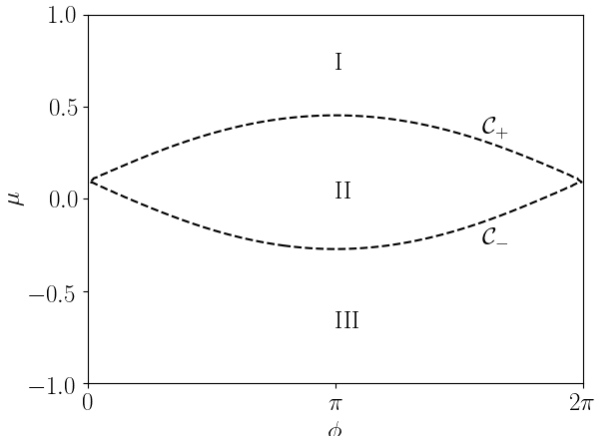

Figure 2. Nomenclature of the two legs of the separatrix $C_\pm$ and three zones of the domain. For both $C_\pm$, we will take the positive direction to be anti-clockwise.

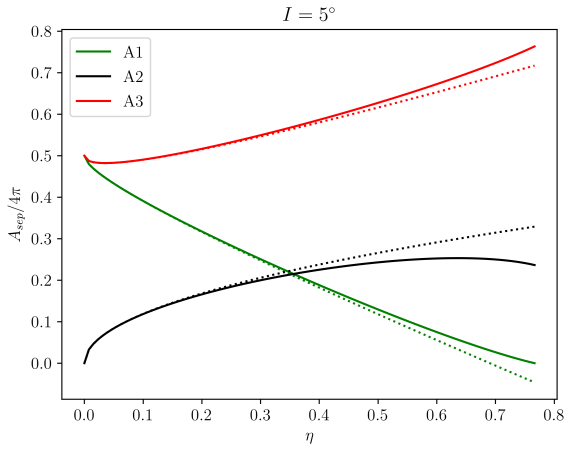

Figure 3. Plot of $A_i(\eta)$ as given by Equation 12. Dotted lines correspond to small η approximations discussed in Section B.

past and future to CS4. Together, these two critical trajectories are referred to as the *separatrix* and divide phase space into three zones. We use notation described in Figure 2.

The area enclosed by the separatrix is known exactly in literature (Henrard & Murigande 1987; Ward & Hamilton 2004):

$$z_0 = \eta \cos I \qquad \chi = \sqrt{-\frac{\tan^3 \theta_4}{\tan I} - 1},$$

$$\rho = \chi \frac{\sin^2 \theta_4 \cos \theta_4}{\chi^2 \cos^2 \theta_4 + 1} \qquad T = 2\chi \frac{\cos \theta_4}{\chi^2 \cos^2 \theta_4 - 1},$$

$$A_2 = 8\rho + 4 \arctan T - 8 z_0 \arctan \frac{1}{\chi}, \tag{12a}$$

$$A_1 = 2\pi (1 - z_0) - \frac{A_2}{2}, \tag{12b}$$

$$A_3 = 2\pi (1 + z_0) - \frac{A_2}{2}. \tag{12c}$$

These are plotted as a function of η in Figure 3.

3 ADIABATIC EVOLUTION

In the truly adiabatic limit, $\epsilon \to 0$; we use $\epsilon = 3 \times 10^{-4}$ in subsection 3.1 and vary ϵ in subsection 3.2. The adiabatic limit is quantified in Millholland & Batygin (2019) to be

$$\dot{\eta} \lesssim \dots \tag{13}$$

3.1 Individual Simulations

In the limit $\eta \to 0$, all trajectories circulate with constant

$$\theta_{sl,f} \equiv \left[\arccos \hat{s} \cdot \hat{l}\right]_{\eta \to 0}. \tag{14}$$

We run simulations that terminate at $\eta = 10^{-5}$ and measure $\theta_{sl,f}$. We vary the initial

$$\theta_{sd,i} \equiv \left[\arccos \hat{s} \cdot \hat{l}_d\right]_{t=0}. \tag{15}$$

While complex at first sight, the outcomes of evolutionary trajectories are only complicated by interactions with the separatrix (as phase space area is conserved otherwise). Adopting the labels in Figure 2, the five dynamical histories we observe in simulations are described by their transitions between regions of phase space:

- $A_2 \to A_1$ — Figure 4.
- $A_2 \to A_3$ — Figure 5.
- $A_3 \to A_1$ — Figure 6.
- $A_3 \to A_2 \to A_1$ — Figure 7.
- $A_3 \to A_3$ — Trivial case, the initial enclosed area is too large to ever experience a separatrix encounter.

3.2 Dynamical Outcomes

In the adiabatic limit, while separatrix encounters induce discontinuous changes in enclosed phase space, the outcomes of these encounters are well understood in pioneering work by Henrard (Henrard 1982; Henrard & Murigande 1987). For a wide range of $\theta_{sd,i}$, we run simulations over a ring of initial conditions at each $\theta_{sd,i}$ and measure the final $\theta_{sl,f}$ values. We can also predict the values of $\theta_{sl,f}$ for each of the dynamical histories as well as their associated probabilities; refer to Section B for details.

4 NONADIABATIC EVOLUTION

Here, we consider ϵ sufficiently large to violate the adiabiticity constraint Equation 13.

4.1 Sample Trajectory

A sample trajectory following in the style of Figure 4 but for $\epsilon = 0.1$ is provided in Figure 9.

4.2 Dynamical Outcomes

A formula for $\theta_{sl,f}$ assuming $\theta_{sd,i} = 0$ initially can be given:

$$\theta_{sl,f}\left(\theta_{sd,i} = 0\right) = \sqrt{\frac{2\pi\Omega}{\epsilon}} \tan I. \tag{16}$$

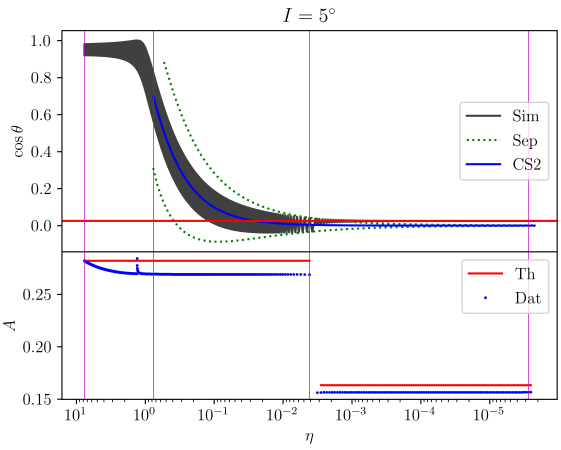

(a) Top: Plot of $\cos\theta(t)$ (grey) over an example simulation. Overlaid are the locations of Cassini State 2 (blue), upper and lower bounds on the separatrix (dashed green), and value of $\theta_{sl,f}$ predicted in the adiabatic limit (horizontal red line). Bottom: Plot of the enclosed separatrix area obtained by integrating the simulated trajectory (blue dots) and fully adiabitic theory (red line). A small blip in the data area arises when the integration area crosses the coordinate singularity at the pole. Vertical red magenta lines denote the four snapshots depicted below; they correspond to the start of the simulation, the appearance of the separatrix, the separatrix encounter and the end of the simulation.

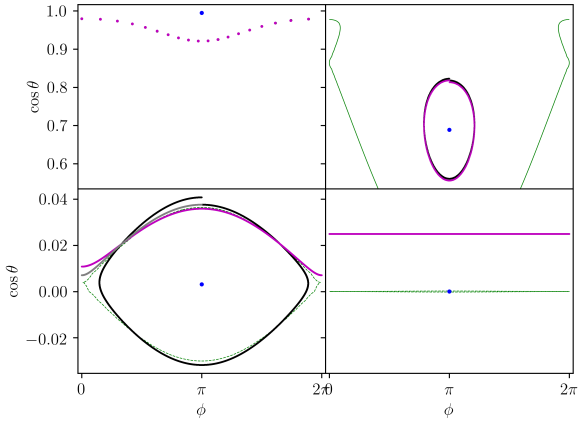

(b) Snapshots in the $(\cos\theta, \phi)$ space of the simulation trajectories for two circulation/libration cycles around the η values depicted above. Cycles are defined by the range of integration used to compute enclosed phase space area. Black dots denote the cycle immediately before the selected η value, magenta dots the cycle immediately after, and grey denotes intermediate points that do not constitute a full cycle. Also labeled are the separatrix (green) and Cassini State 2 (blue).

Figure 4. Fiducial simulation following the $A_2 \rightarrow A_1$ transition.

We can naively generalize this by recognizing that any nonzero $\theta_{sd,i}$ manifests as obliquity variations as $\hat{s}$ librates about $\hat{l}_d$, and these oscillations are "frozen in" when the disk dissipates. Thus,

$$\theta_{sl,f}\left(\theta_{sd,i}\right) \in \sqrt{\frac{2\pi\Omega}{\epsilon}} \tan I \pm \theta_{sd,i}. \tag{17}$$

We present the results of simulations for using $\epsilon = 0.3$ in Figure 10.

4.3 Transition from Adiabaticity

The agreement of Equation 16 at fixed I for varying ϵ is shown in Figure 11. Note that $\epsilon \rightarrow 0$ recovers the adiabatic regime.

An example of an intermediate value $\epsilon = 10^{-2}$ between Figure 8 and Figure 10 is shown in

TODO compare to Equation 13.

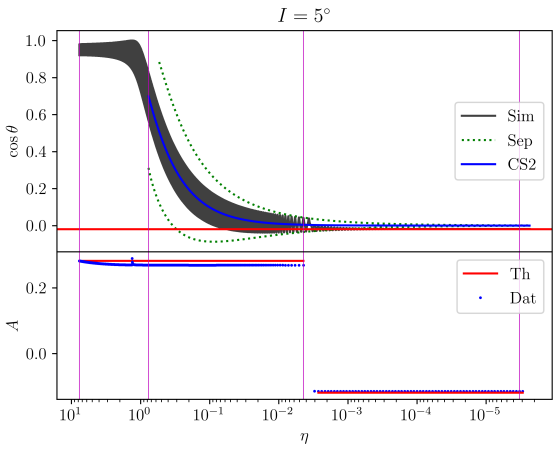

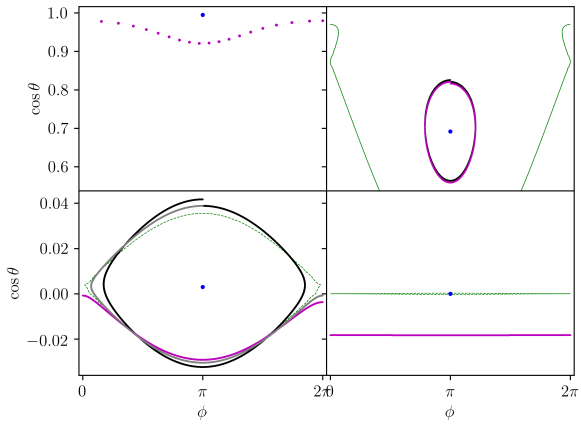

Figure 5. Same as Figure 4 but for the $A_2 \rightarrow A_3$ history.

REFERENCES

Anderson K. R., Lai D., 2018, Monthly Notices of the Royal Astronomical Society, 480, 1402
Henrard J., 1982, Celestial Mechanics and Dynamical Astronomy, 27, 3
Henrard J., Murigande C., 1987, Celestial Mechanics, 40, 345
Millholland S., Batygin K., 2019, The Astrophysical Journal, 876, 119
Ward W. R., Hamilton D. P., 2004, The Astronomical Journal, 128, 2501

APPENDIX A: VARIATION WITH I

Plots of Figure 8 but for $I = 10°, I = 20°$.

APPENDIX B: CALCULATION OF TRANSITION PROBABILITIES

Semi-analytic calculation probabilities, including naive line.

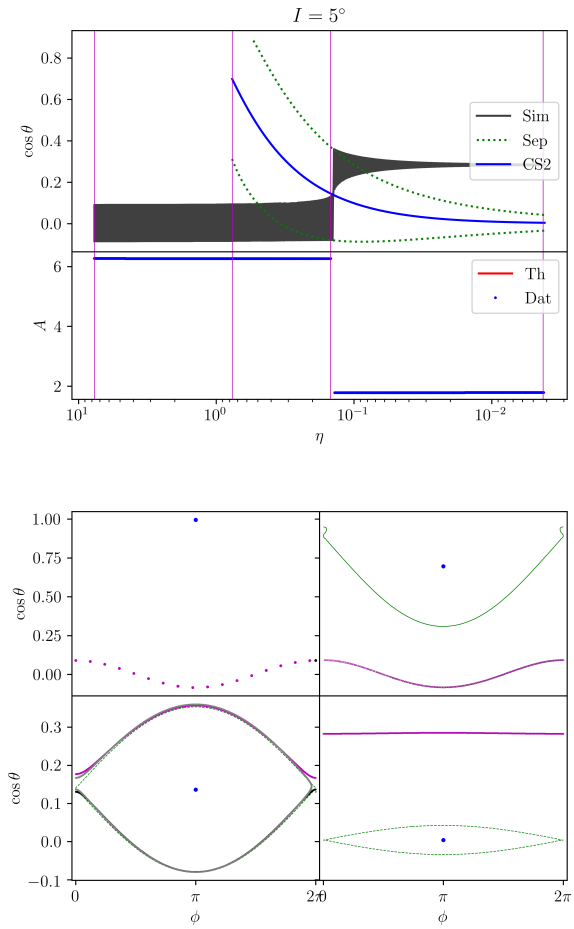

Figure 6. Same as Figure 4 but for the $A_3 \to A_1$ history. TODO finish final areas plot.

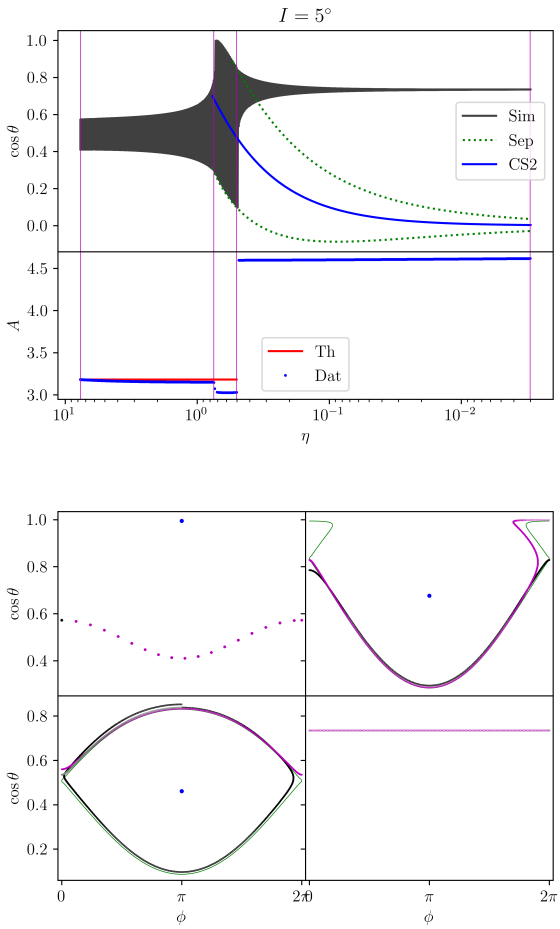

Figure 7. Same as Figure 4 but for the $A_3 \to A_2 \to A_1$ history. The second snapshot, instead of depicting the appearance of the separatrix, captures the first of the two separatrix crossings. TODO finish final areas plot.

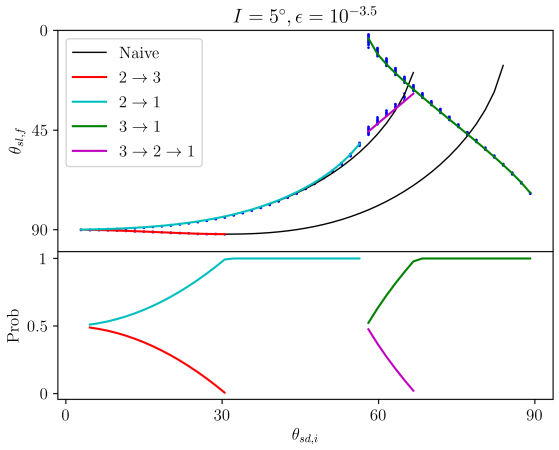

Figure 8. Top: $\theta_{sl,f}$ $(\theta_{sd,i})$, overlaid with semi-analytic predictions of the $\theta_{sl,f}$ for each of the four nontrivial dynamical histories in colored lines. Bottom: Semi-analytic probabilities of each of the dynamical histories for each $\theta_{sd,i}$.

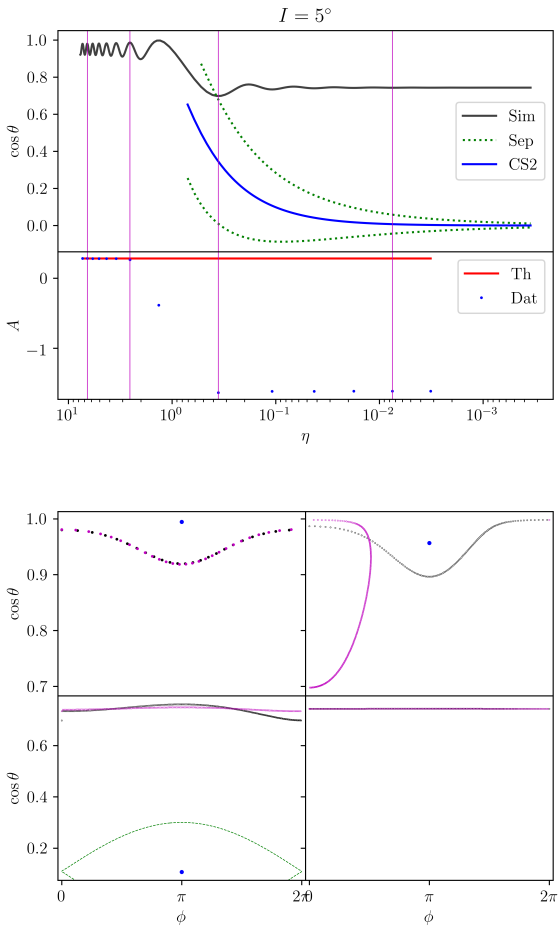

Figure 9. Same as Figure 9 but for a non-adiabatic $\epsilon = 0.1$.

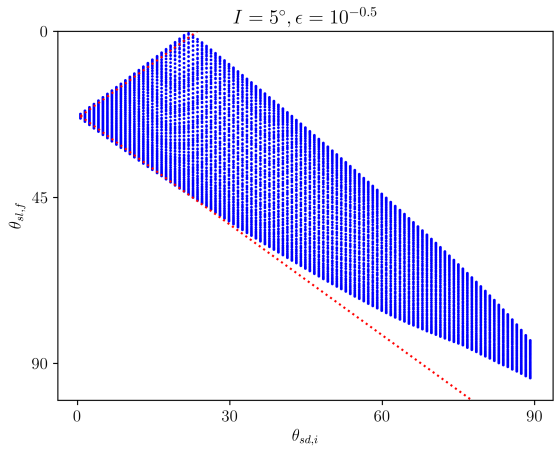

Figure 10. $\theta_{sl,f}\left(\theta_{sd,i}\right)$ at $\epsilon = 0.3$, firmly in the non-adiabatic regime. Note the clear double-valuedeness has disappeared, as have distinct dynamical histories. The red dotted line presents the analytical prediction given by Equation 17.

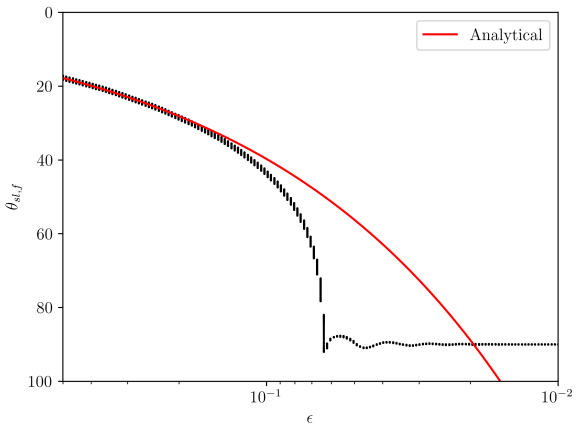

Figure 11. Plot of $\theta_{sl,f}\left(\theta_{sd,i} = 0\right)$ as a function of ϵ, where $I = 5°$. Overplotted in the red line is Equation 16, which is in good agreement for $\epsilon \gtrsim 0.1$ the non-adiabatic regime, while $\theta_{sl,f} \approx 90°$ in the adiabatic regime.

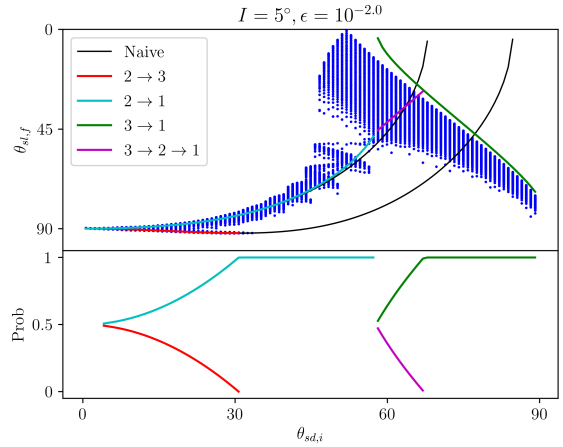

Figure 12. Intermediate ϵ used in between those of Figure 8 and Figure 10. Noticeable "freezing-in" of the obliquity variations over libration cycles is still visible, but the shapes of the adiabatic dynamical trajectories are beginning to appear.